Temperature-dependent permittivity of silver and implications for thermoplasmonics

Marzia Ferrera,[1] Michele Magnozzi,[1,2] Francesco Bisio,[3,*] and Maurizio Canepa[1]
[1]*OptMatLab, Dipartimento di Fisica, Università di Genova, via Dodecaneso 33, I-16146 Genova, Italy*
[2]*Istituto Nazionale di Fisica Nucleare, Sezione di Genova, via Dodecaneso 33, I-16146 Genova, Italy*
[3]*CNR-SPIN, Corso Perrone 24, I-16152 Genova, Italy*

(Received 12 August 2019; published 17 October 2019)

Silver is an extremely appealing metal for plasmonics due to its very low optical losses in the visible and near-ultraviolet range and its relatively low reactivity. Within the emerging field of thermoplasmonics, where light-metal interactions are exploited to generate heat on the nanometric scale, knowledge of temperature-dependent complex permittivities of plasmonic materials is indispensable. We extracted the temperature-dependent complex permittivity of silver ε_{Ag} by spectroscopic ellipsometry under high-vacuum conditions. For rising T, we observed an increase of the free-electron contribution to the imaginary part of the permittivity $\mathrm{Im}[\varepsilon_{Ag}]$ and a temperature-dependent absorption band splitting off the interband absorption edge in the 320–360-nm range. Around 340 nm the *relative* increase of $\mathrm{Im}[\varepsilon_{Ag}]$ at 600 K with respect to its room-temperature value is around 500%. In order to understand the implications of this behavior on silver thermoplasmonics, we computed the temperature-dependent extinction efficiency of oblate Ag ellipsoids with localized plasmon resonance within the 320–360-nm range. We predict that dramatic damping of the plasmon resonance occurs for increasing temperature, possibly leading to intriguing self-limiting effects in Ag thermoplasmonics.

DOI: 10.1103/PhysRevMaterials.3.105201

I. INTRODUCTION

Silver is a noble metal widely appreciated and exploited for outstanding properties such as low electrical resistivity and low optical losses in the visible (VIS)-light regime [1–3]. The latter property is widely exploited in plasmonics, where Ag yields localized surface plasmon resonances (LSPRs) with the highest quality factor among all metals [2–7]. This has promoted the widespread use of Ag whenever experimental requirements such as sharp LSPRs or ultrahigh field-enhancement factors are a must [8–14].

Given its huge relevance for applications in optics and photonics, the complex permittivity of bulk Ag ε_{Ag} has been widely investigated from both theoretical and experimental points of view [15–21]. For photon energies below 3.9 eV the optical response of Ag is well described in the framework of the free-electron model. For higher energies, interband transitions come into play, with a subsequent increase of $\mathrm{Im}[\varepsilon_{Ag}]$ in correspondence with the sharp absorption edge, while $\mathrm{Re}[\varepsilon_{Ag}]$ assumes positive values in the near-ultraviolet range [15,19,22,23]. It is important to notice that, as for almost any material, sample preparation issues, contamination effects, and measurement protocols vary from case to case, so that, even for room-temperature data, somewhat different values of ε_{Ag} are reported in the literature, as highlighted, e.g., in Ref. [20].

The recent rise of thermoplasmonics, where plasmonic metallic structures are exploited as localized heat generators at the nanometer scale [4,24–26], has brought renewed interest to the temperature-dependent optical properties of plasmonic metals [27,28]. Indeed, assessing the thermoplasmonic response of metallic nanostructures mandatorily requires knowledge of their temperature-dependent complex dielectric permittivity $\varepsilon(T)$ [26,27,29]. The $\varepsilon_{Ag}(T)$ for bulk and thin-film silver has been investigated in the distant and more recent past [22,23,30–33]; recent investigations, however, either especially focused on the free-electron part of the spectrum [23] or addressed also the interband region but were partly hindered by sample purity issues [22,30–32].

In this work, we present a study of the temperature-dependent complex dielectric permittivity of silver $\varepsilon_{Ag}(T)$ spanning the ultraviolet (UV) interband range and the near-infrared (NIR) intraband spectral region. The study was performed by means of spectroscopic ellipsometry (SE) under high-vacuum (HV) conditions in order to prevent any kind of contamination and covered the 298–610 K temperature range. In the NIR we observed that the dielectric function of Ag varies in a smooth fashion as a function of temperature, resulting in a gradual, expected rise of the free-electron contribution (so-called Drude tail) [23]. In the UV, we witnessed the appearance of a marked absorption band in the 320–360-nm wavelength interval, which splits off from the room-temperature (RT) interband edge with rising T [29]. Around $\lambda = 340$ nm, such a feature yields a 500% relative increase of the optical dissipation upon a few-hundred-degree variation of temperature, potentially yielding strong temperature-dependent plasmonic effects in aptly designed Ag nanostructures.

II. EXPERIMENT

The sample was an optically thick and morphologically flat polycrystalline Ag film, deposited by molecular beam

*francesco.bisio@spin.cnr.it

 ©2019 American Physical Society

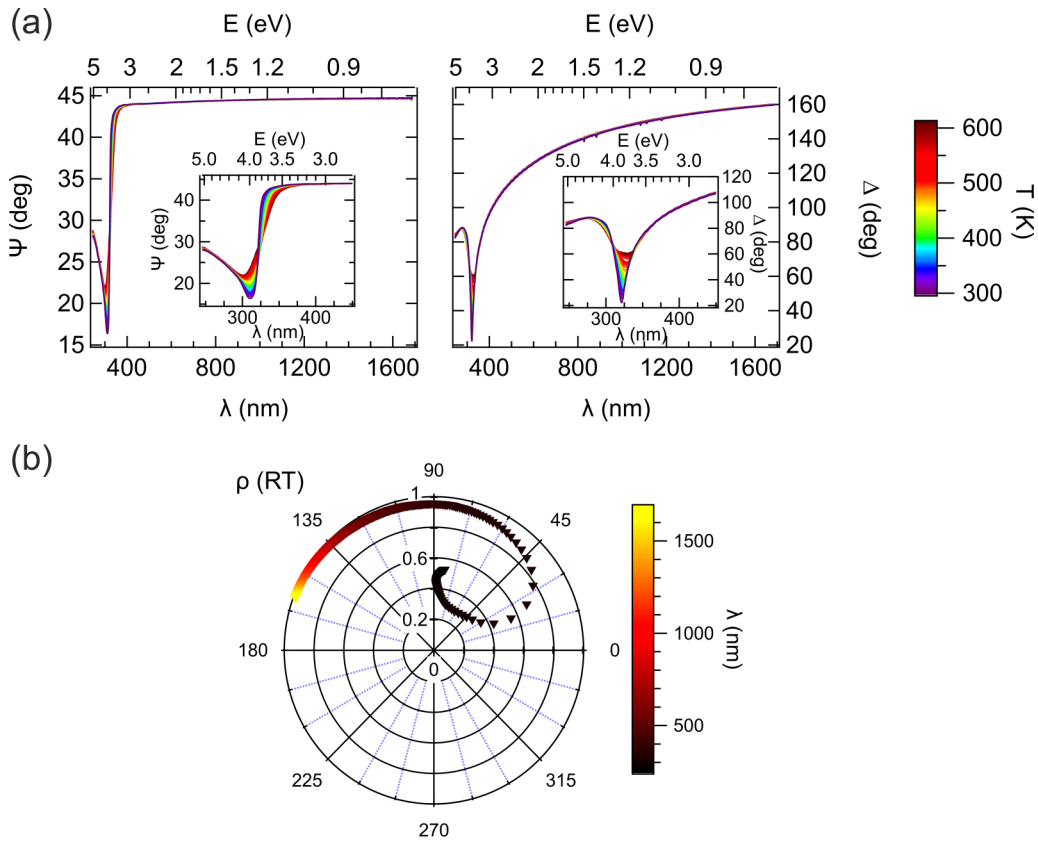

FIG. 1. (a) SE $\Psi(\lambda)$, $\Delta(\lambda)$ spectra vs temperature. The sample temperature is indicated by the color scale. The temperature difference between adjacent traces is around 12.5 K. Insets: zoom over the 245–450-nm wavelength range. (b) Polar plot of the complex function $\rho(\lambda)$ at RT.

epitaxy on a silicon wafer with a native oxide substrate within a HV chamber with base pressure $p \approx 2 \times 10^{-9}$ mbar. The film thickness was about 150 nm, enough to consider it semi-infinite from an optical point of view. After deposition, the sample was transferred into a dedicated roll-on/roll-off HV chamber (base pressure $\approx 10^{-7}$ mbar), specially designed to fit between the arms of a J.A. Woollam M-2000 spectroscopic ellipsometer and endowed with a heating stage to perform real-time, *in situ* SE at variable temperature [28,34]. The sample was briefly exposed to the atmosphere during the transfer. SE was performed in the $\lambda = 245$–1700 nm wavelength range, at an angle of incidence $\theta_i = 66^\circ$. The unavoidable influence of optical viewports was compensated by appropriate algorithms [34,35]. The sample was annealed at $T = 610$ K in the chamber, and SE measurements were acquired during the subsequent cooling ramp, setting the sample at various temperatures between 610 K and RT. The pressure did not exceed 10^{-6} mbar during the whole experiment.

The wavelength-dependent Ψ and Δ ellipsometric spectra are defined according to

$$\rho = \frac{r_p}{r_s} = \frac{|r_p|e^{i\delta_p}}{|r_s|e^{i\delta_s}} = \frac{|r_p|}{|r_s|}e^{i(\delta_p-\delta_s)} = \tan\Psi e^{i\Delta}, \qquad (1)$$

where $r_{p,s}$ are the p, s-polarized complex Fresnel reflection coefficients of the system [36].

In Fig. 1(a), we report the $\Psi(\lambda)$ and $\Delta(\lambda)$ spectra of Ag as a function of temperature T. The Ψ spectra are flat throughout the VIS-NIR spectral range at $\Psi \approx 45^\circ$ before showing a very marked dip around 310 nm and increasing again towards lower wavelengths. For increasing T, we observe that the edge of the Ψ plateau gradually smears, while the dip in Ψ becomes significantly shallower and blueshifts to 300 nm.

The Δ spectra monotonously decrease with decreasing wavelength from the NIR, where Δ reads $\approx 160^\circ$, to the VIS range, before exhibiting a very narrow dip around 320 nm and increasing again for lower λ. For growing temperature, Δ remains nearly unchanged in the VIS-NIR region, whereas the UV dip gradually gets shallower. The dips in Ψ and Δ are roughly located in the spectral region where interband absorption sets in, at a photon energy of about 3.9 eV [37].

The SE spectra that we report are representative of a clean and flat Ag film; under these conditions, the dielectric function can be simply extracted from the SE spectra according to

$$\langle\varepsilon(\lambda)\rangle = \varepsilon_{Ag} = \sin^2\theta_i\left[1 + \tan^2\theta_i\left(\frac{1-\rho(\lambda)}{1+\rho(\lambda)}\right)^2\right]. \qquad (2)$$

Here, we notice that, at large wavelengths, $\rho \to -1$ in the complex plane (as $\tan\Psi \to 1$ and $\Delta \to 180^\circ$), as represented in the polar plot of Fig. 1(b) (RT data). Under these conditions, the expression $(\frac{1-\rho}{1+\rho})^2$ diverges, yielding a very large sensitivity of ε_{Ag} upon small changes of Ψ and Δ. At this stage even very slight deviations from optimal behavior of optical viewports in Ψ and Δ can have a large influence on ε_{Ag}. Now, the temperature dependence of ε_{Ag} in the NIR range has been thoroughly addressed in previous articles [23]. However,

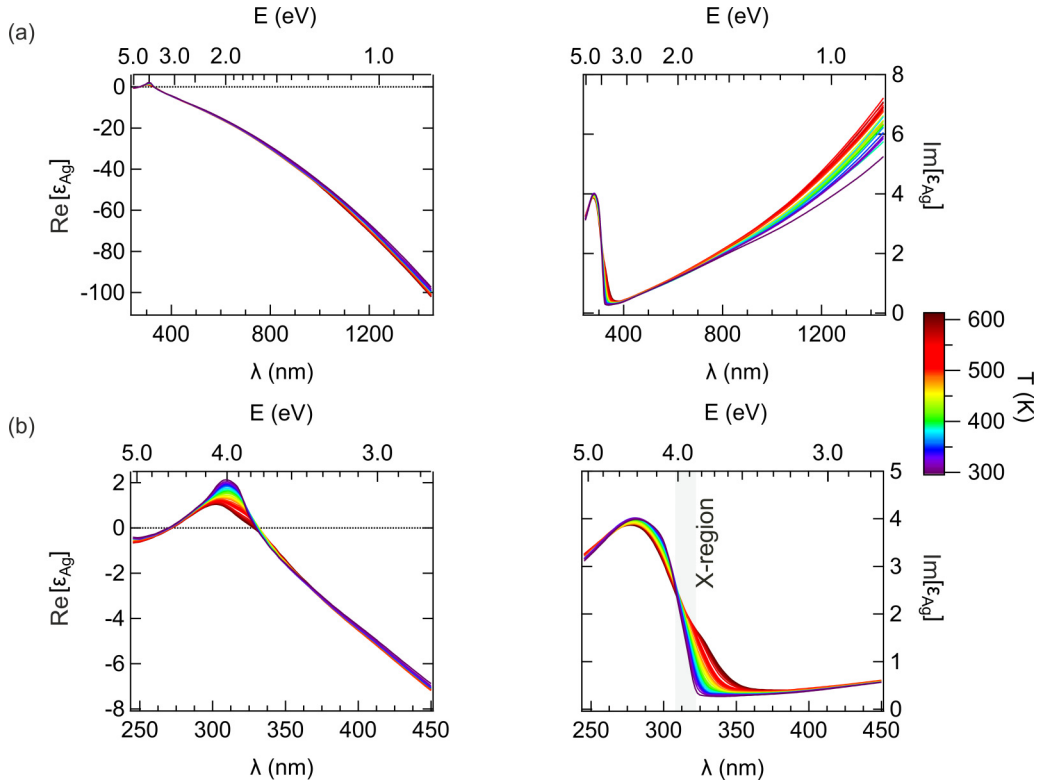

FIG. 2. (a) Real (left) and imaginary (right) parts of ε_{Ag} in the 245–1450-nm spectral range from RT (violet) to HT (dark red) extracted from the SE experimental data of Fig. 1. (b) Zoom of the 245–450-nm spectral range (2.8–5.1 eV).

Ref. [23] did not fully investigate the interband range. For this reason, in this paper we forgo the NIR range and focus mostly on the UV-VIS part, reporting ε_{Ag} in only the 245–1450-nm range.

III. DISCUSSION

A. Temperature-dependent dielectric permittivity

In Fig. 2(a), we present the real and imaginary parts of ε_{Ag} for temperatures ranging from RT to 610 K in the 245–1450-nm (0.9–5.1-eV) spectral range (see Supplemental Material [38]). Let us focus on RT data first. The ε_{Ag} clearly shows two distinct contributions: the free-electron part dominates the VIS-NIR spectral range, whereas the interband transitions represent the major contribution below 400 nm. We will first discuss the RT values and assess their compatibility with reported values and then move on to describe the temperature dependence of ε_{Ag}.

In the free-electron part, our data at RT are fully compatible with the recent data of Ref. [23] for *e*-beam-deposited polycrystalline Ag film and of Ref. [19] for template-stripped Ag films. It is worth noting that in the intraband spectral range, Im[ε] is strongly influenced by both grain size and surface roughness, as shown in detail in Ref. [39]: this can explain minor variations in the Drude tail from sample to sample.

The Drude contribution smoothly and regularly decreases with increasing photon energy right up to the interband threshold, indicative of a contamination-free surface [20]. Thus, the thin oxide layer that might have formed during the sample transfer is efficiently decomposed by the HV annealing. The minimum of Im[ε_{Ag}] is located at $E \approx 3.7$ eV and reads 0.26, similar to that in Refs. [19,23] and in agreement with previous values [16,40–42].

Moving towards the high-energy part of the spectrum, interband transitions set in. Im[ε_{Ag}] reaches the maximum value of 4 around 4.4 eV, compatible with the values reported in the literature [15,19,43,44], and correspondingly, Re[ε_{Ag}] becomes positive and reaches values greater than 2 around 4.0 eV, similar to those in Refs. [19,43].

Moving to the temperature-dependent data, we notice a gradual rise of the Drude tail in Im[ε_{Ag}] with increasing T due to the enhanced electronic scattering by phonons [23,45]. In the NIR, Re[ε_{Ag}] increases in absolute value with increasing T, possibly due to the increase of plasma frequency with T [23,46]. It is worth noting that ε_{Ag} exhibits very weak changes with T all across the VIS regime (400–700 nm), seemingly at variance with data by Reddy *et al.* [23] while in agreement with Ref. [31], although the latter data report higher Im[ε_{Ag}] throughout this range.

Zooming into the interband region [Fig. 2(b)], interesting spectral details can be appreciated. Indeed, we observe that an absorption peak progressively splits off from the interband edge with increasing T, yielding an increased optical dissipation in the 320–360-nm range. Meanwhile, in the 260–310-nm range, the increasing T leads to a decrease of Im[ε_{Ag}], so that there exists a narrow spectral window [highlighted in light gray in Fig. 2(b)], labeled the X region, where Im[ε_{Ag}] is almost T invariant [29,31]. The invariance of Im[ε_{Ag}] in the X region has its roots in the invariance of the energy gap of the electronic bands involved in the interband transitions

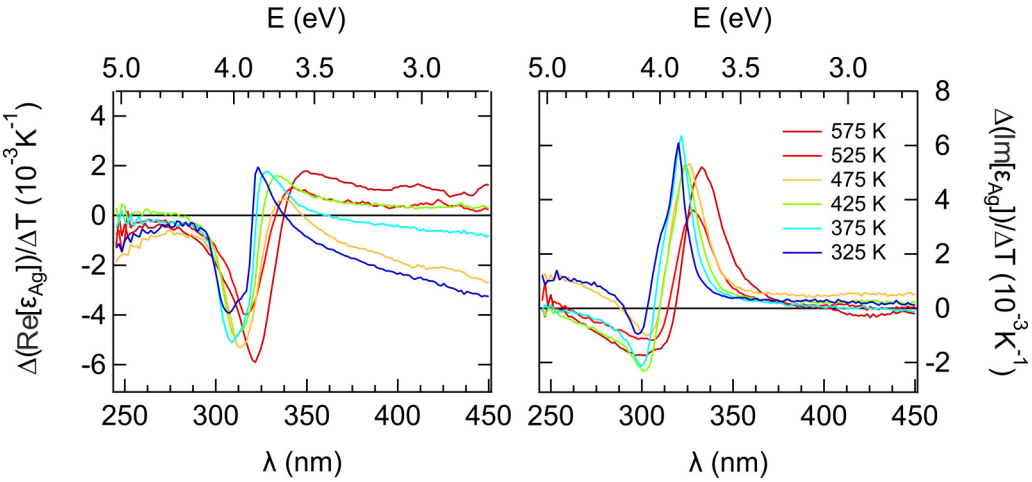

FIG. 3. Spectral dependence of $\Delta\mathrm{Re}[\varepsilon_{Ag}]/\Delta T$ and $\Delta\mathrm{Im}[\varepsilon_{Ag}]/\Delta T$ in the 245–450-nm wavelength interval.

at this energy, which undergo approximately identical energy shifts vs T [29,31,32]. These variations are reflected also in the T dependence of $\mathrm{Re}[\varepsilon_{Ag}]$, where a localized decrease vs T in the spectral region around 320 nm is observed. The appearance of the extra-absorption feature in $\mathrm{Im}[\varepsilon_{Ag}]$ around the 320–360-nm range is related to the interband transition between conduction bands in the proximity of the interband critical point $L_{4^-} \rightarrow L_{4^+}$: the energy gap between the conduction bands involved in this transition is strongly temperature dependent, and it is reflected in the variation of the dielectric response of the system upon heating [22,30,31].

In order to better highlight the temperature gradients in the optical response, in Fig. 3, we plot $\Delta\varepsilon_{Ag}/\Delta T$ (real and imaginary parts) in the 245–450-nm spectral region extracted from the data of Fig. 2. The data were obtained by taking the difference between sets of $\varepsilon_{Ag}(T)$ curves 50 K apart from each other in order to limit the noise levels. The temperature of each $\Delta\varepsilon_{Ag}/\Delta T$ curve is the average temperature between the two $\varepsilon_{Ag}(T)$ curves employed to calculate the derivative. Both sets of curves assume typical values on the order of 10^{-3} K^{-1}, in agreement with previous results [22,47–49]. Clearly, the major feature of the $\Delta\varepsilon_{Ag}/\Delta T$ curves is localized across the interband threshold, reflecting the unusual temperature evolution of ε_{Ag} in that range. We suggest that these data can represent a new benchmark for exploitation in thermoplasmonics models [48] or comparison with theoretical models of out-of-equilibrium dielectric functions [50].

B. Implications for thermoplasmonics

Interestingly, we notice that the extra absorption appearing in the 320–360-nm range [30] features two relevant characteristics. The first is that it falls within a region where the corresponding RT values of $\mathrm{Im}[\varepsilon_{Ag}]$ are extremely low, below 0.3, so that the *relative* increase of $\mathrm{Im}[\varepsilon_{Ag}]$ with T is almost fivefold (i.e., *a 500% increase*). The second is that this region is potentially still within reach of LSPRs of Ag nanostructures. The combination of these facts envisages a potentially interesting thermoplasmonic response of Ag nanostructures, where the quantitative evaluation of the temperature dependence of the Ag dielectric function becomes pivotal [47–49].

In order to evaluate the consequences of the Ag thermo-optical response for plasmonics, we performed a simple calculation of the temperature-dependent extinction coefficients of Ag nanoellipsoids. In order to obtain a sizable LSPR in the wavelength interval of 320–360 nm, we chose a silver oblate nanospheroid, with a high aspect ratio, in order to have transverse plasmonic resonances in the UV. We chose the long semiaxes $a_x = a_y = 20$ nm and short semiaxis $a_z = 5$ nm [Fig. 4(a)] in order to have neither a size-dependent LSPR redshift nor strong finite-size effects on ε_{Ag}. We calculated its extinction efficiency Q_{ext} (defined as the ratio between the extinction cross section and the projected area of the nanospheroid) within the modified long-wavelength approximation (MLWA) [51,52], including finite-size corrections to the free-electron part of ε_{Ag} [53,54]. Due to the system symmetry, we yield different Q_{ext} spectra for electric field oriented along the long ellipsoid semiaxis, the so-called longitudinal mode (LM), and along the short semiaxis, which corresponds to the transverse mode (TM). The depolarization factors employed in the calculations are $L_x = L_y = 0.1482$ and $L_z = 0.7036$, respectively [55].

In Fig. 4(b), we present the calculated Q_{ext} at $T = 298$ K (blue line) and at $T = 610$ K (red line) for an Ag ellipsoid immersed in vacuum ($\varepsilon_M = 1$) for the LM mode (thin line) and the TM mode (thick line). At RT, the LM peak falls within the VIS range, peaking at about 2.9 eV, while the TM excitation falls within the interband transitions region, with a narrow resonant peak at $E \approx 3.7$ eV. The temperature evolution of Q_{ext} is amazingly different for LM and TM resonances. Indeed, the LM peak undergoes a small blueshift of about 4 nm and a tiny intensity drop, while its width is approximately unchanged, whereas the TM peak is strongly affected by the extra-absorption band at HT in the 320–360-nm interval, which causes a huge (fourfold) intensity drop and a resonance broadening. These are variations much larger than most thermoplasmonic responses.

In order to address whether these effects persist under more realistic conditions, we calculated the RT and high-T

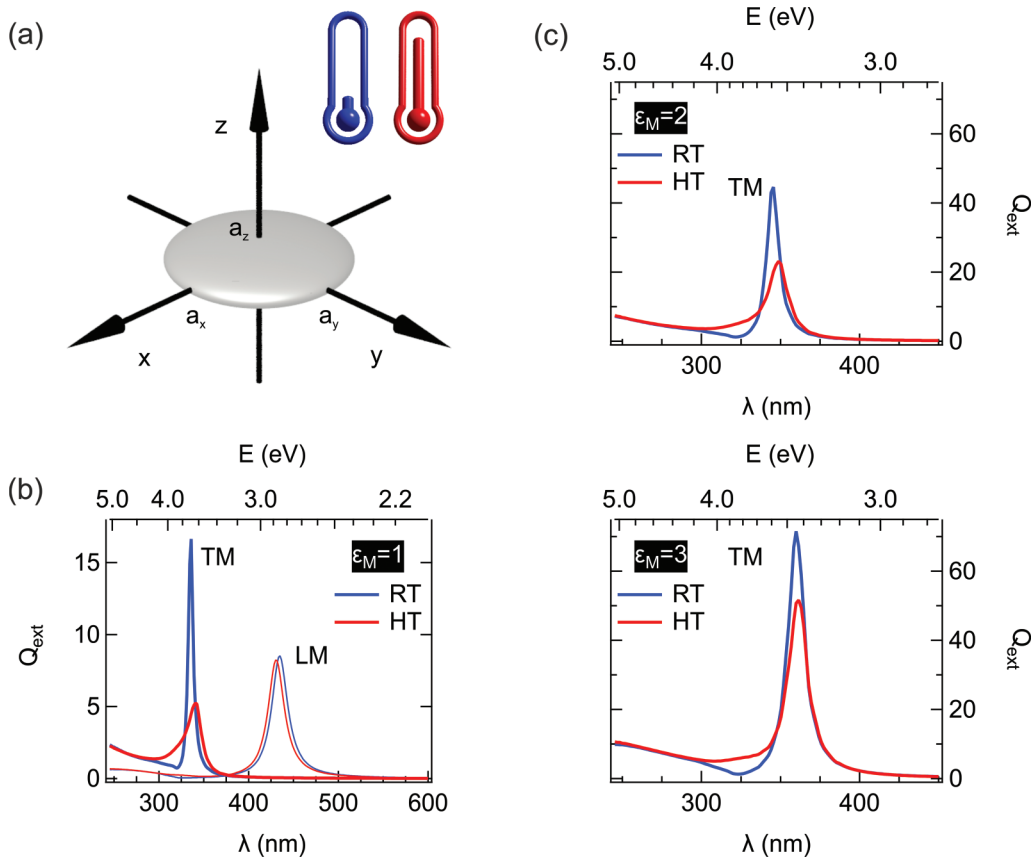

FIG. 4. (a) Geometry of the oblate silver nanospheroid (aspect ratio $a_x/a_z = 4$). (b) Extinction efficiency for light polarized along the x axis (LM, thin line) and along the z axis (TM, thick line) at 298 K (blue) and 610 K (red). (c) Extinction efficiency of the Ag nanospheroid embedded in transparent media with increasing Re[ε_m] for light polarized along the z axis (TM) at 298 K (blue) and 610 K (red).

extinction efficiencies of the TM for Ag ellipsoids embedded within transparent hosts with Re[ε_m] = 2 and Re[ε_m] = 3 [Fig. 4(c)]. The LSPR gradually redshifts with increasing permittivity of the host, and the differences between RT and high-T gradually fade, while still remaining sizable up to $\varepsilon_m = 3$. This suggests that large thermoplasmonic effects should indeed be observable in experimentally accessible conditions; furthermore, these experiments, if performed, could provide interesting information about the potential role of finite-size effects in the thermo-optical response of Ag compared to the present calculations performed by means of bulk values of ε_{Ag}.

IV. CONCLUSION

We have investigated the thermo-optical response of Ag by means of *in situ* spectroscopic ellipsometry from RT to 610 K in the 245–1450-nm λ range. The study was performed under high-vacuum conditions in order to prevent Ag contamination. For increasing T we observed an increase of the Drude tail in Im[ε_{Ag}] due to the electron-scattering enhancement and a corresponding decrease in Re[ε_{Ag}] due to the plasma frequency increase with T [23,45,46]. In the near-UV region, we observed a T-dependent absorption band gradually splitting off the main interband edge [22,30,31] such that, around 340 nm, the *relative* increase of Im[ε_{Ag}] at 610 K with respect to its RT value is around 500%.

In order to test the potential impact of this effect within the emerging field of thermoplasmonics, we employed these data to calculate the extinction efficiency of oblate Ag ellipsoids within the MLWA approximation, applying finite-size corrections to the free-electron part of the experimental ε_{Ag}. We showed that the T-dependent absorption band strongly dampens and broadens the LSPR for Ag nanostructures with resonance in the near-UV range. More generally, our data show that an accurate evaluation of the temperature dependence of the Ag dielectric function is mandatory to correctly model the thermo-optical properties of Ag-based plasmonic systems. The temperature dependence of Q_{ext} is also of interest because of its potential of self-limited heating of aptly designed Ag nanostructures. Indeed, as T rises, the extinction efficiency gradually drops, allowing a subtle equilibrium between extinction and dissipation to be found at temperature values significantly different with respect to simple expectations based on the RT dielectric permittivity.

ACKNOWLEDGMENTS

We acknowledge the support from the Ministero dell'Istruzione, dell'Università e della Ricerca (PRIN NEWLI, No. 2015CL3APH) and from the Compagnia di San Paolo (project PanLab).

[1] B. Wiley, Y. Sun, and Y. Xia, Acc. Chem. Res. **40**, 1067 (2007).
[2] E. C. L. Ru and P. G. Etchegoin, in *Principles of Surface-Enhanced Raman Spectroscopy*, edited by E. C. L. Ru and P. G. Etchegoin (Elsevier, Amsterdam, 2009), pp. 121–183.
[3] M. Rycenga, C. M. Cobley, J. Zeng, W. Li, C. H. Moran, Q. Zhang, D. Qin, and Y. Xia, Chem. Rev. **111**, 3669 (2011).
[4] A. Lalisse, G. Tessier, J. Plain, and G. Baffou, J. Phys. Chem. C **119**, 25518 (2015).
[5] M. Gorkunov, V. Artemov, S. Yudin, and S. Palto, Photonics Nanostruct.: Fundam. Appl. **12**, 122 (2013).
[6] T. W. Ebbesen, H. J. Lezec, H. F. Ghaemi, P. A. Thio, and T. Wolff, Nature (London) **391**, 667 (1998).
[7] A. Kubo, K. Onda, H. Petek, Z. Sun, Y. S. Jung, and H. K. Kim, Nano Lett. **5**, 1123 (2005).
[8] E. Hao and G. C. Schatz, J. Chem. Phys. **120**, 357 (2004).
[9] A. Tao, P. Sinsermsuksakul, and P. Yang, Nat. Nanotechnol. **2**, 435 (2007).
[10] A. R. Tao, D. P. Ceperley, P. Sinsermsuksakul, A. R. Neureuther, and P. Yang, Nano Lett. **8**, 4033 (2008).
[11] M. J. Mulvihill, X. Y. Ling, J. Henzie, and P. Yang, J. Am. Chem. Soc. **132**, 268 (2010).
[12] A. Boltasseva and H. A. Atwater, Science **331**, 290 (2011).
[13] J. Harra, J. Mäkitalo, R. Siikanen, M. Virkki, G. Genty, T. Kobayashi, M. Kauranen, and J. M. Mäkelä, J. Nanopart. Res. **14**, 870 (2012).
[14] A. S. Baburin, A. M. Merzlikin, A. V. Baryshev, I. A. Ryzhikov, Y. V. Panfilov, and I. A. Rodionov, Opt. Mater. Express **9**, 611 (2019).
[15] P. B. Johnson and R. W. Christy, Phys. Rev. B **6**, 4370 (1972).
[16] D. J. Nash and J. R. Sambles, J. Mod. Opt. **43**, 81 (1996).
[17] E. D. Palik, *Handbook of Optical Constants of Solids* (Academic, Boston, 1998).
[18] K. Stahrenberg, T. Herrmann, K. Wilmers, N. Esser, W. Richter, and M. J. G. Lee, Phys. Rev. B **64**, 115111 (2001).
[19] H. U. Yang, J. D'Archangel, M. L. Sundheimer, E. Tucker, G. D. Boreman, and M. B. Raschke, Phys. Rev. B **91**, 235137 (2015).
[20] Y. Jiang, S. Pillai, and M. Green, Opt. Express **23**, 2133 (2015).
[21] Y. Jiang, S. Pillai, and M. Green, Sci. Rep. **6**, 30605 (2016).
[22] P. Winsemius, F. F. van Kampen, H. P. Lengkeek, and C. G. van Went, J. Phys. F **6**, 1583 (1976).
[23] H. Reddy, U. Guler, K. Chaudhuri, A. Dutta, A. V. Kildishev, V. M. Shalaev, and A. Boltasseva, ACS Photonics **4**, 1083 (2017).
[24] G. Baffou, R. Quidant, and C. Girard, Appl. Phys. Lett. **94**, 153109 (2009).
[25] E. C. Garnett, W. Cai, J. J. Cha, F. Mahmood, S. T. Connor, M. Greyson Christoforo, Y. Cui, M. D. McGehee, and M. L. Brongersma, Nat. Mater. **11**, 241 (2012).
[26] G. Baffou, *Thermoplamonics: Heating Metal Particles Using Light* (Cambridge University Press, Cambridge, UK, 2017).
[27] H. Reddy, U. Guler, A. V. Kildishev, A. Boltasseva, and V. M. Shalaev, Opt. Mater. Express **6**, 2776 (2016).
[28] M. Magnozzi, M. Ferrera, L. Mattera, M. Canepa, and F. Bisio, Nanoscale **11**, 1140 (2019).
[29] P. Winsemius, *Temperature Dependence of the Optical Properties of Au and Ag* (Drukkerij J. H. Pasmans, Den Haag (NL), 1973).
[30] H. G. Liljenvall and A. G. Mathewson, J. Phys. C **3**, S341 (1970).
[31] S. T. Sundari, S. Chandra, and A. K. Tyagi, J. Appl. Phys. **114**, 033515 (2013).
[32] S. T. Sundari, K. Srinivasu, S. Dash, and A. Tyagi, Solid State Commun. **167**, 36 (2013).
[33] Y.-J. Chen, M.-C. Lee, and C.-M. Wang, Jpn. J. Appl. Phys. **53**, 08MG02 (2014).
[34] M. Magnozzi, F. Bisio, and M. Canepa, Appl. Surf. Sci. **421**, 651 (2017).
[35] *Guide to Using WVASE 32: Spectroscopic Ellipsometry Data Acquisition and Analysis Software* (J. A. Woollam Co., Lincoln, USA, 2008).
[36] H. Fujiwara, *Spectroscopic Ellipsometry: Principles and Applications* (Wiley, Chichester, England, 2007).
[37] P. K. Jain, Angew. Chem., Int. Ed. **53**, 1197 (2014).
[38] See Supplemental Material at http://link.aps.org/supplemental/10.1103/PhysRevMaterials.3.105201 for complete data sets as a function of wavelength and temperature, for use in numerical analyses.
[39] D. E. Aspnes, E. Kinsbron, and D. D. Bacon, Phys. Rev. B **21**, 3290 (1980).
[40] M. Otter, Z. Phys. **161**, 539 (1961).
[41] C. v. Fragstein and H. Kampermann, Z. Phys. **173**, 39 (1963).
[42] T. Hollstein, U. Kreibig, and F. Leis, Phys. Status Solidi B **82**, 545 (1977).
[43] H.-J. Hagemann, W. Gudat, and C. Kunz, J. Opt. Soc. Am. **65**, 742 (1975).
[44] G. Leveque, C. G. Olson, and D. W. Lynch, Phys. Rev. B **27**, 4654 (1983).
[45] A. Alabastri, S. Tuccio, A. Giugni, A. Toma, C. Liberale, G. Das, F. D. Angelis, E. D. Fabrizio, and R. P. Zaccaria, Materials **6**, 4879 (2013).
[46] C.-Y. Young, J. Phys. Chem. Solids **30**, 2765 (1969).
[47] T. Stoll, P. Maioli, A. Crut, N. Del Fatti, and F. Vallée, Eur. Phys. J. B **87**, 260 (2014).
[48] M. Gandolfi, A. Crut, F. Medeghini, T. Stoll, P. Maioli, F. Vallée, F. Banfi, and N. Del Fatti, J. Phys. Chem. C **122**, 8655 (2018).
[49] M. G. Silva, D. C. Teles-Ferreira, L. Siman, C. R. Chaves, L. O. Ladeira, S. Longhi, G. Cerullo, C. Manzoni, A. M. de Paula, and G. Della Valle, Phys. Rev. B **98**, 115407 (2018).
[50] A. M. Brown, R. Sundararaman, P. Narang, W. A. Goddard, and H. A. Atwater, Phys. Rev. B **94**, 075120 (2016).
[51] K. L. Kelly, E. Coronado, L. L. Zhao, and G. C. Schatz, J. Phys. Chem. B **107**, 668 (2003).
[52] K. D. Ko and K. C. Toussaint, Jr., J. Quant. Spectrosc. Radiat. Transfer **110**, 1037 (2009).
[53] H. Hövel, S. Fritz, A. Hilger, U. Kreibig, and M. Vollmer, Phys. Rev. B **48**, 18178 (1993).
[54] L. Anghinolfi, R. Moroni, L. Mattera, M. Canepa, and F. Bisio, J. Phys. Chem. C **115**, 14036 (2011).
[55] C. Louis and O. Pluchery, *Gold Nanoparticles for Physics, Chemistry and Biology*, 2nd ed. (World Scientific, Singapore, 2017).